Electronic Supplementary Material (ESI) for Dalton Transactions

<Electronic Supplementary Information>

Direct anion effects on the formation of 1D, 2D, and 3D coordination polymers: construction and properties of copper(II) complexes containing 1,3,5-tris(isonicotinoyloxyethyl)cyanurate

Woosik Hong, Haeri Lee, Tae Hwan Noh and Ok-Sang Jung*

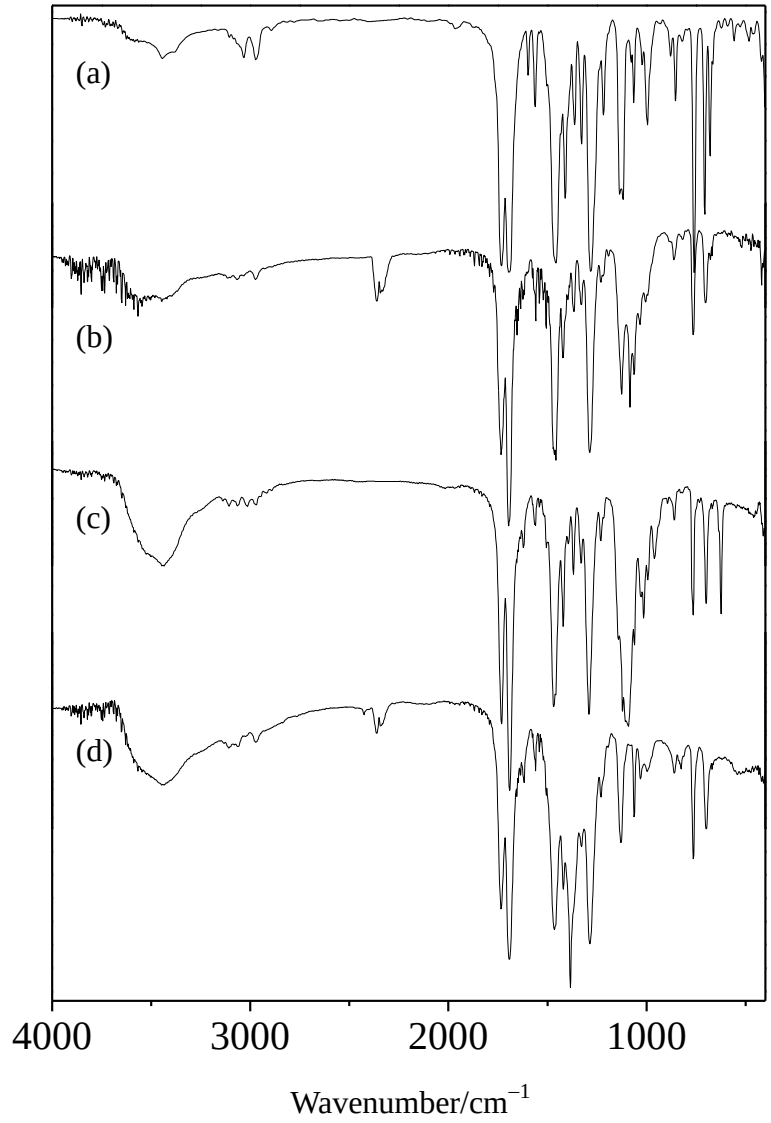

Fig. S1 IR data of L (a), $[Cu(BF_4)(L)_2(H_2O)](BF_4)\cdot 2H_2O$ (b), $[Cu(ClO_4)(L)(Me_2SO)_2](ClO_4)\cdot 2CH_2Cl_2$ (c), and $[Cu_2(NO_3)_4(L)_2(CH_3OH)]\cdot 2CH_2Cl_2\cdot 2CH_3OH$ (d).

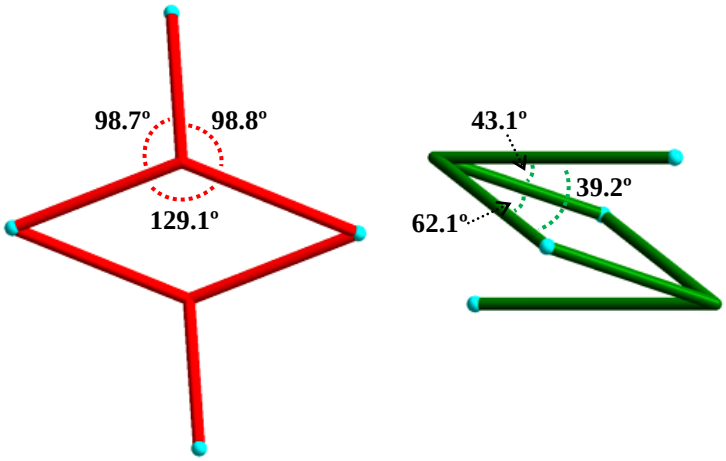

Fig. S2 Schematic diagrams showing the difference in conformation between L of the layered moiety (red) and the bridging moiety (green) for $[Cu_2(NO_3)_4(L)_2(CH_3OH)]\cdot 2CH_2Cl_2\cdot 2CH_3OH$.

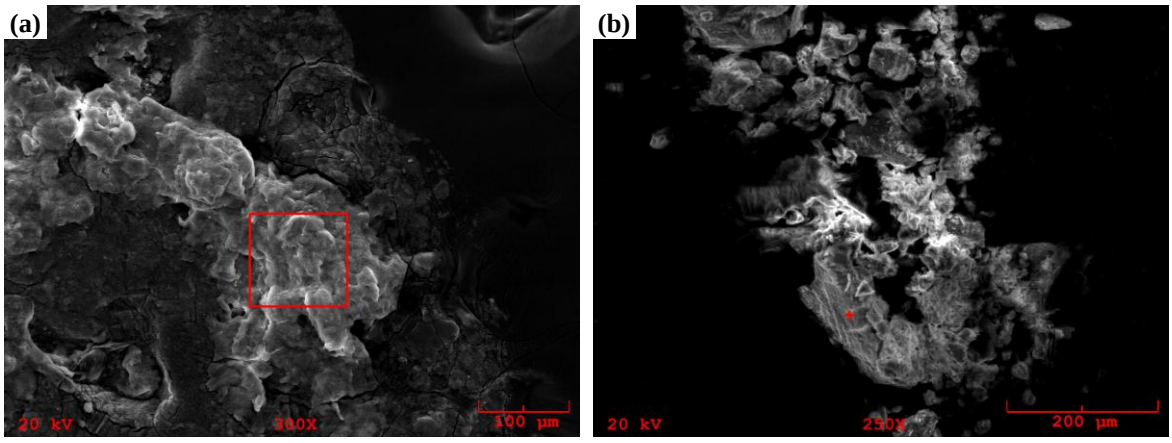

Element	Atomic% (**a**)	Atomic% (**b**)
B	3.499	3.896
C	50.971	54.150
N	10.880	15.058
O	25.187	19.499
F	5.611	3.959
Cl	2.451	2.181
Cu	1.401	1.257
	100.000	100.000

Fig. S3 SEM images (top) and SEM-EDX data (bottom) for the anion exchanged species, $[Cu(BF_4)(L)_2(H_2O)](ClO_4)$ (a) and $[Cu(ClO_4)(L)(Me_2SO)_2](BF_4)$ (b).

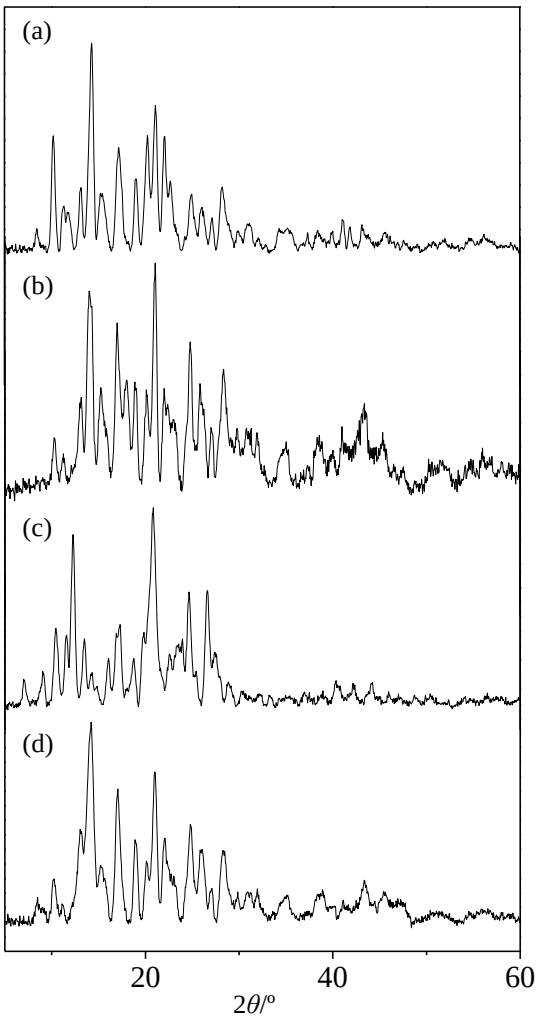

Fig. S4 Powder XRD data showing the anion exchanges: $[Cu(BF_4)(L)_2(H_2O)](BF_4)\cdot 2H_2O$ crystal (a) and the anion exchanged species $[Cu(BF_4)(L)_2(H_2O)](ClO_4)$ after anion exchange with three equivalents of $NaClO_4$ (b); $[Cu(ClO_4)(L)(Me_2SO)_2](ClO_4)\cdot 2CH_2Cl_2$ crystal (c) and the anion exchanged species $[Cu(ClO_4)(L)(Me_2SO)_2](BF_4)$ after anion exchange with three equivalents of $NaBF_4$ (d).

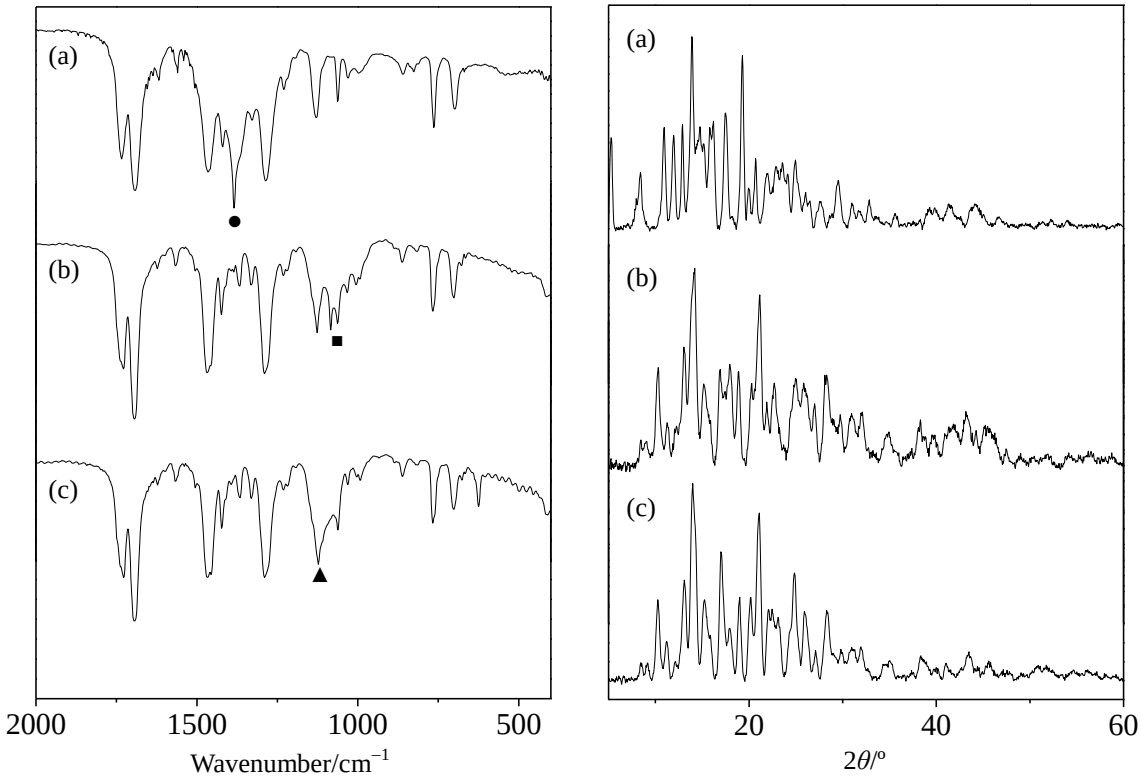

Fig. S5 IR spectra (left) and powder XRD data (right) of $[Cu_2(L)_2(CH_3OH)(NO_3)_4]\cdot 2CH_2Cl_2\cdot 2CH_3OH$ (a) and the anion exchanged species $[Cu_2(BF_4)_4(L)_2(CH_3OH)]$ (b) and $[Cu_2(ClO_4)_4(L)_2(CH_3OH)]$ (c). Circle, square, and triangle indicate the IR bands corresponding to NO_3^-, BF_4^- and, ClO_4^-, respectively.

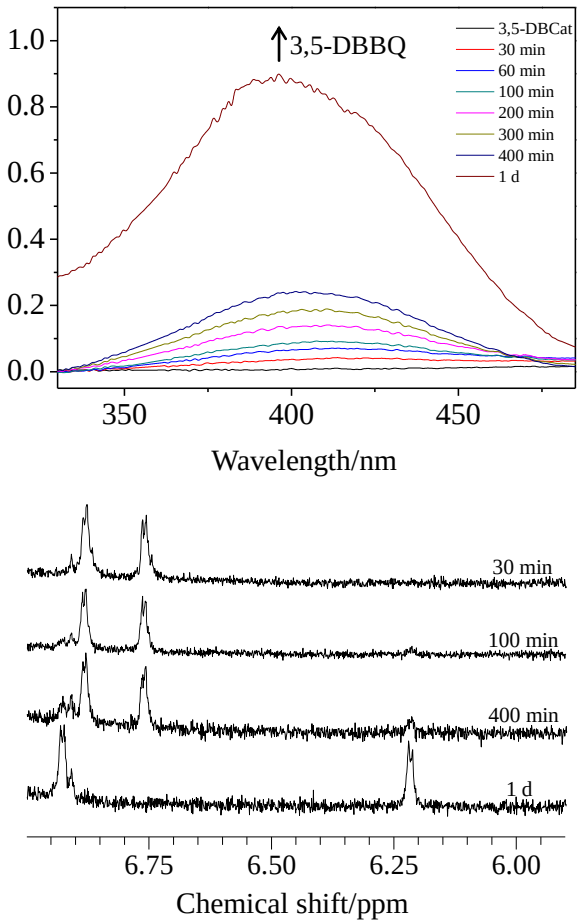

Fig. S6 UV spectra (in chloroform, top) and partial ^{1}H NMR spectra (bottom) and showing oxidation of 3,5-di-*tert*-butylcatechol (3,5-DBCat) with 0.2 mol% $[Cu(BF_4)(L)_2(H_2O)](BF_4)\cdot 2H_2O$ catalysts at 40 ºC.

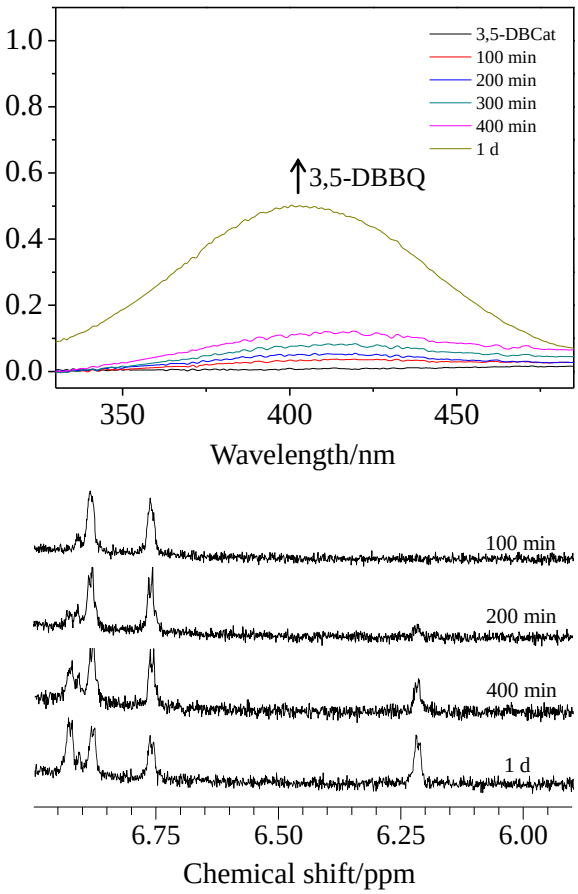

Fig. S7 UV spectra (in chloroform, top) and partial ^{1}H NMR spectra (bottom) showing oxidation of 3,5-di-*tert*-butylcatechol (3,5-DBCat) with 0.2 mol% $[Cu(ClO_4)(L)(Me_2SO)_2](ClO_4)\cdot 2CH_2Cl_2$ catalysts at 40 ºC.

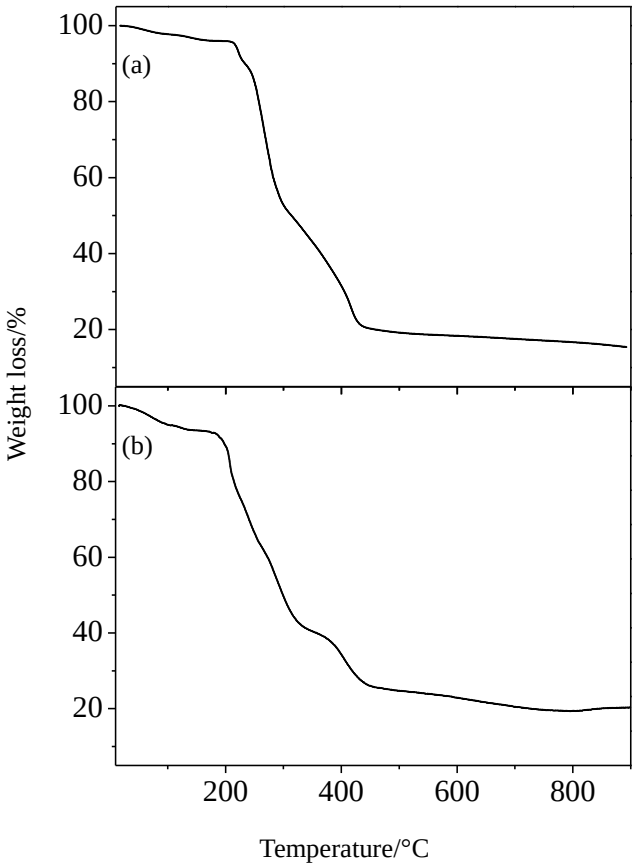

Fig. S8 TGA curves of $[Cu(BF_4)(L)_2(H_2O)](BF_4)\cdot 2H_2O$ (a) and $[Cu_2(NO_3)_4(L)_2(CH_3OH)]\cdot 2CH_2Cl_2\cdot 2CH_3OH$ (b).

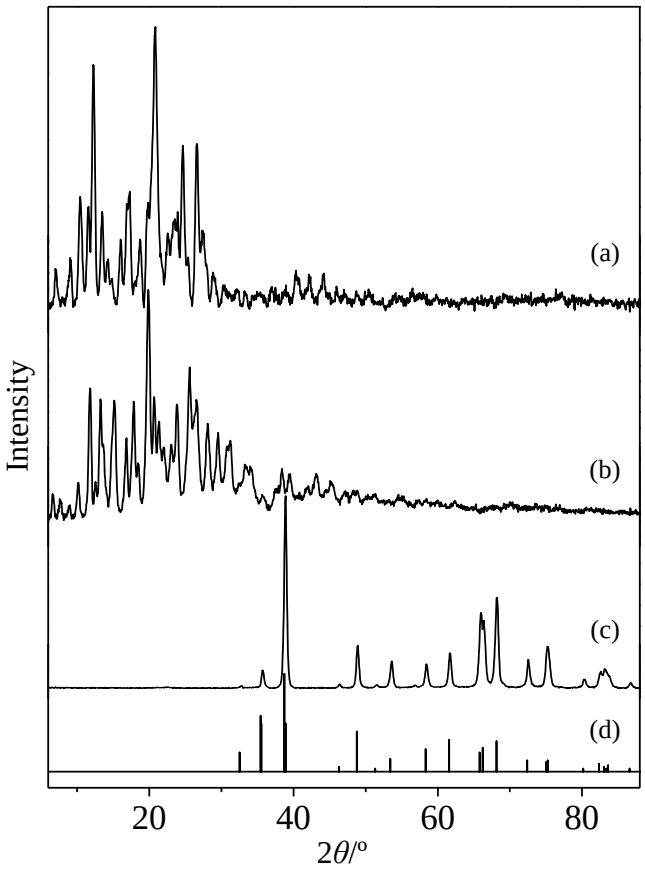

Fig. S9 Powder XRD patterns for $[Cu(ClO_4)(L)(Me_2SO)_2](ClO_4)\cdot 2CH_2Cl_2$ (a) and the calcined samples at 200 ºC for 1 h (b) and at 600 ºC for 2 h (c). (d) represents the reference pattern of CuO from the ICDD database (PDF no. 05-0661).

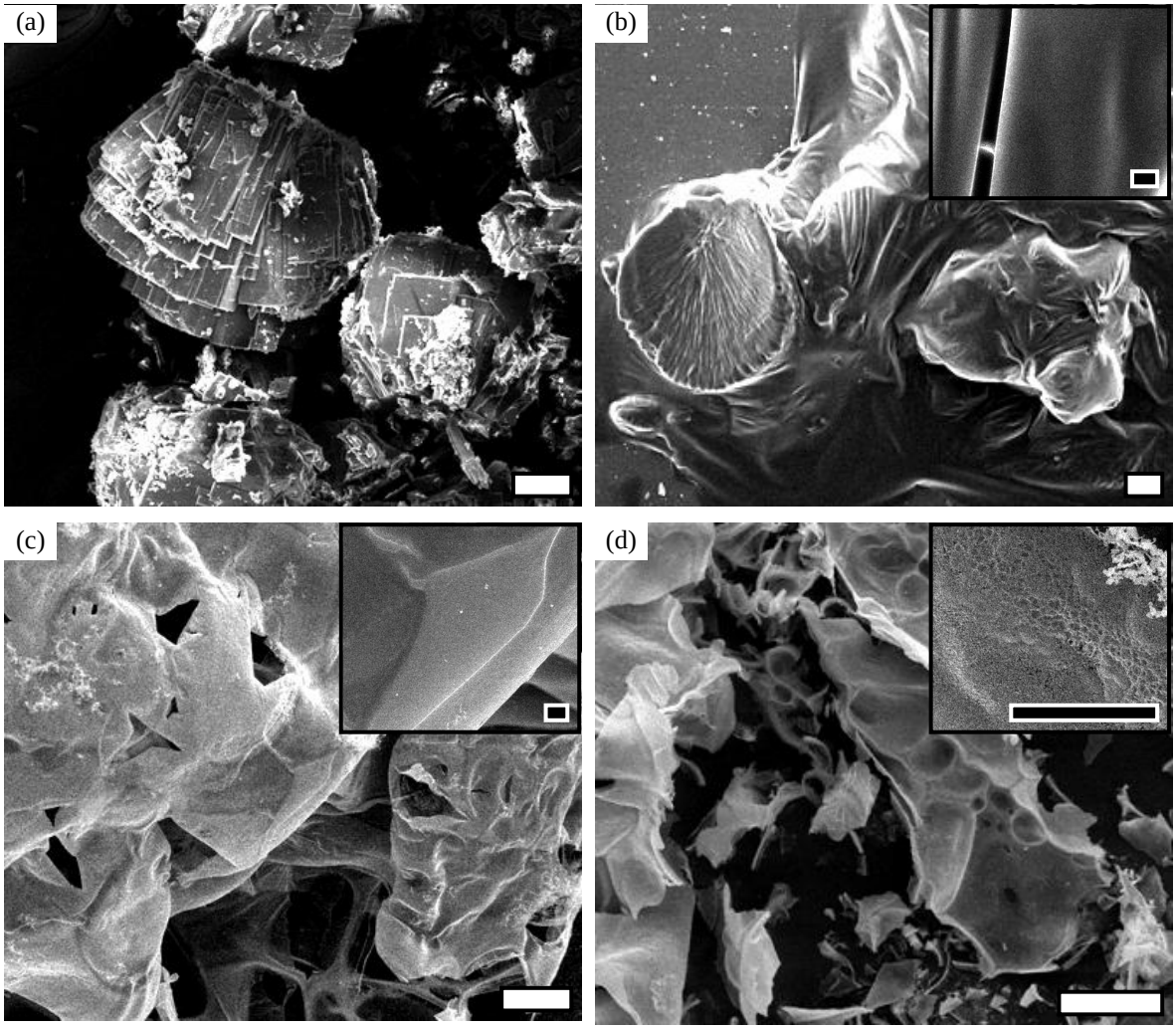

Fig. S10 Temperature-dependent morphology change of $[Cu(BF_4)(L)_2(H_2O)](BF_4)\cdot 2H_2O$ (left): bare crystal (a), calcination at 200 ºC for 1 h (b), 400 ºC for 1 h (c), and 600 ºC for 2 h (d). Inset: magnified images. White bar = 100 μm; black bar = 10 μm.

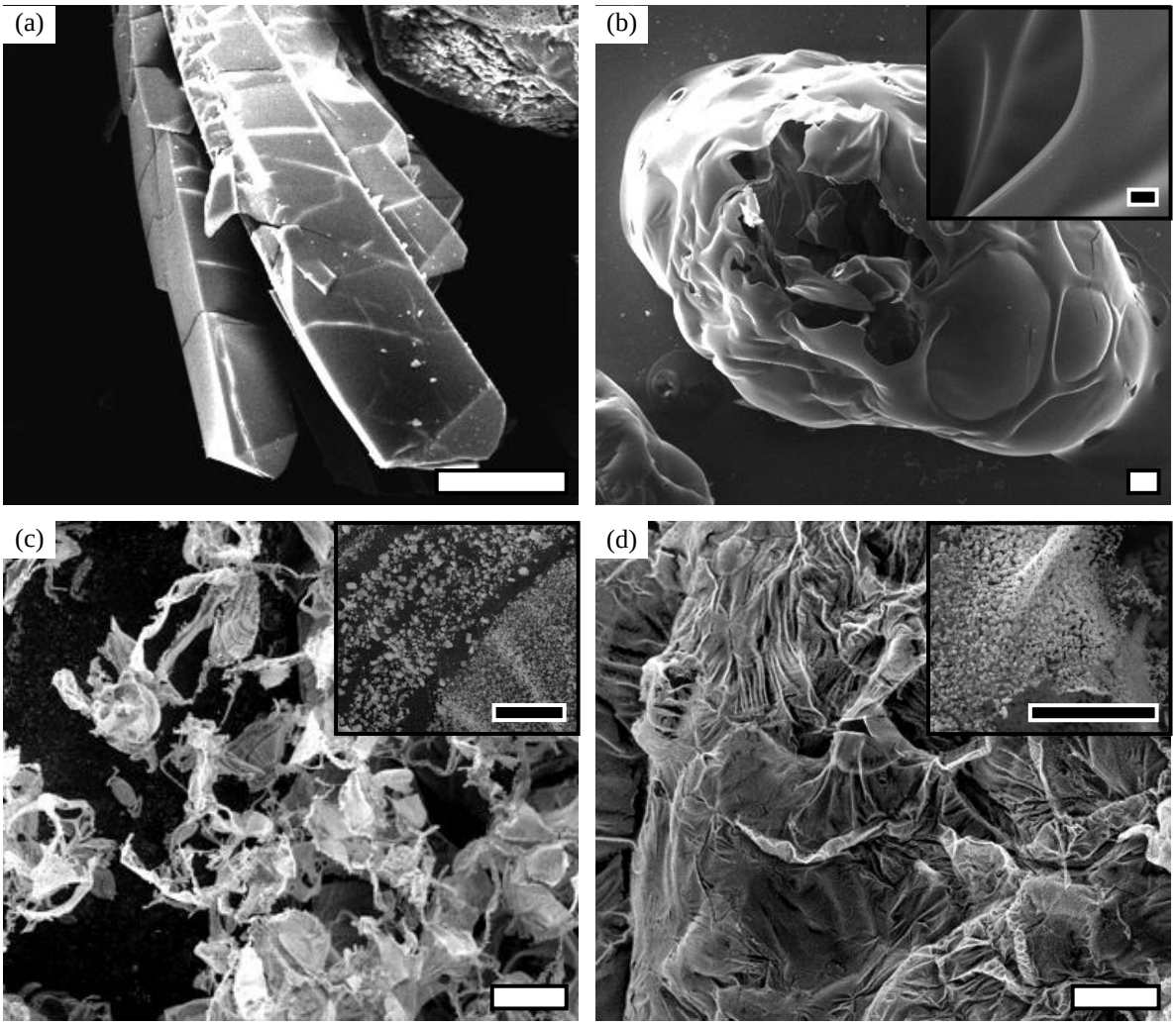

Fig. S11 Temperature-dependent morphology change of $[Cu_2(NO_3)_4(L)_2(CH_3OH)]\cdot 2CH_2Cl_2\cdot 2CH_3OH$: bare crystal (a), calcination at 200 ºC for 1 h (b), 400 ºC for 1 h (c), and 600 ºC for 2 h (d). Inset: magnified images. White bar = 100 μm; black bar = 10 μm.